Original Article

Effects of octane boosters on the formation of oxygenated primary organic aerosol in low-temperature combustion

Omar El Hajj[a], Anna G. Conroy[b], Chase K. Glenn[a], Brandon Rotavera[a,c], and Rawad Saleh[a]

[a]School of Environmental, Civil, Agricultural, and Mechanical Engineering, University of Georgia, Athens, Georgia, USA;

[b]Department of Physics, University of Georgia, Athens, Georgia, USA

[c]Department of Chemistry, University of Georgia, Athens, Georgia, USA

CONTACT Author (1): Rawad Saleh rawad@uga.edu School of Environmental, Civil, Agricultural, and Mechanical Engineering, University of Georgia, 302 E. Campus Rd., i-STEM-1 Building, Athens, GA, 30602 USA.

CONTACT Author (2): Brandon Rotavera rotavera@uga.edu School of Environmental, Civil, Agricultural, and Mechanical Engineering, University of Georgia, 302 E. Campus Rd., i-STEM-1 Building, Athens, GA, 30602 USA.

ABSTRACT

We have previously demonstrated that *n*-alkanes that exhibit two-stage ignition also exhibit two-stage primary organic aerosol (POA) formation. The first-stage POA, or oxygenated POA (OxyPOA), forms via alkylperoxy radical chemistry that involves sequential oxidation reactions of cyclic ethers generated during first-stage ignition. Here, we perform controlled-combustion experiments and chemical kinetics simulations to investigate the effect of octane boosters (toluene, ethanol, and 2,5-dimethylfuran (DMF)) on OxyPOA emissions from *n*-heptane as the primary fuel. Both ethanol and DMF exhibited synergistic blending for OxyPOA suppression (i.e. suppressed OxyPOA beyond what is calculated based on molar displacement of *n*-heptane), in concordance with their reported synergistic blending for research octane number (RON), while toluene exhibited antagonistic blending for OxyPOA suppression. DMF was the most effective at suppressing OxyPOA formation, also in concordance with its reported efficiency at scavenging OH radicals produced during first-stage ignition. This finding indicates that DMF, an advanced drop-in biofuel with superior octane boosting characteristics, also has the added benefit of reducing aerosol pollution. Chemical analysis using electrospray ionization Fourier-transform ion cyclotron resonance mass spectrometry showed that the reactions of the octane boosters with OH radicals formed OxyPOA molecules via pathways different from those produced from *n*-heptane. These reactions are similar to the OH-oxidation reactions that produce secondary organic aerosol (SOA) in the atmosphere. This suggests that, contrary to current understanding of atmospheric aerosols, some POA emitted from low-temperature combustion (i.e. OxyPOA) can be chemically similar to SOA.

1. Introduction

Certain fuels, including *n*-alkanes larger than ethane and classes of oxygenated biofuels, such as ethers, exhibit two-stage ignition (Ju, 2021; Ribaucour et al., 2000; Rotavera & Taatjes, 2021; Westbrook, 2000) owing to temperature-dependent chain-branching mechanisms. First-stage ignition, which is governed by the formation of peroxy (RO_2) radicals, occurs below ~850 K and leads to chain-branching as a result of second-O_2-addition reactions with initial carbon-centered radicals. Second-stage ignition occurs at temperatures higher than 1000 K, resulting from chain-branching steps including $H + O_2 \rightarrow OH + O$. The two stages are separated by a negative temperature coefficient (NTC) region in which fuel reactivity decreases with increasing temperature (Westbrook, 2000). First-stage ignition is implicated in engine knock (Leone et al., 2015; Westbrook et al., 2018; Wheeler et al., 1948). Furthermore, first-stage ignition and the associated low-temperature heat release (LTHR) is essential for the operation of advanced compression-ignition (ACI) engines (Waqas et al., 2019). Fuel reactivity is conventionally quantified using the research octane number (RON) (Splitter et al., 2016; Szybist et al., 2021), where lower RON reflects higher fuel reactivity, or more prominent two-stage ignition behavior.

We have recently shown that fuels that exhibit two-stage ignition also exhibit two-stage aerosol formation (O El Hajj et al., 2021; Omar El Hajj et al., 2024). The second-stage aerosol forms via the extensively studied soot-formation route (Michelsen, 2017; Wang, 2011) that involves growth and clustering of polycyclic aromatic hydrocarbons (PAHs) and aliphatic species aided by radical chain reactions involving resonance-stabilized radicals (Johansson et al., 2018). The soot-formation process is highly temperature dependent. Incipient soot, comprised of organic molecules, forms at relatively low second-stage combustion temperatures (Michelsen, 2017). As the temperature increases, the incipient soot undergoes a series of dehydrogenation and clustering, eventually forming mature soot, which is comprised of mostly elemental carbon (Russo et al., 2015; Tregrossi & Ciajolo, 2010). Therefore, for relatively low second-stage combustion temperatures, the emitted aerosol is organic and is classified as primary organic aerosol (POA) in atmospheric science terminology. We refer to this POA as second-stage POA (Omar El Hajj et al., 2024). First-stage POA forms via pathways different from those of soot, and have only been recently discovered

(Omar El Hajj et al., 2024). The building blocks of first-stage POA are cyclic ethers produced in the gas phase coincident with OH in a chain-propagating step from ring-closure of hydroperoxyl (QOOH) radicals, which are derived from RO_2 radicals of the fuel. In subsequent oxidation steps, cyclic ether intermediates (e.g. 2-methyltetrahydrofuran) can undergo H-abstraction. Following O_2-addition to the cyclic ether radical, the adduct (a cyclic ether-peroxy radical) can act as an abstractor leading to a hydroperoxide (ROOH). When H-abstraction from the (cyclic) ROOH occurs, specifically involving labile tertiary hydrogen from the same carbon atom on which the –OOH group resides, a carbon-centered radical is produced wherein the electron is localized adjacent to the –OOH group. Following a barrierless decomposition step coincident with OH, the species forms a carbonyl group (e.g. 2-methyl-tetrahydrofuran-3-one). The repeated pattern, initialized by the formation of a cyclic ether, H-abstraction, O_2-addition, formation of cyclic ROOH, and carbonyl formation thereafter leads to the formation of highly oxygenated species with decreased volatilities. These species constitute monomers that condense and form aerosol particles and undergo molecular growth by oligomerization in the particle phase, thus further decreasing their volatilities and promoting further monomer condensation. To distinguish it from traditional POA (i.e. second-stage POA, or incipient soot), we refer to first-stage POA as oxygenated POA (OxyPOA) (Omar El Hajj et al., 2024).

The two-stage POA formation has implications on emissions from spark-ignition engines at cold-start conditions. We have previously observed signatures of OxyPOA in the emissions of a spark-ignition engine operated at simulated cold-start conditions (Omar El Hajj et al., 2024), which was attributed to a portion of the emissions experiencing temperature histories within the first-stage ignition range due to the cold cylinder walls. The two-stage POA formation also has implications on emissions from ACI engines that rely on low-temperature combustion (LTC). ACI technologies aim to reduce NO_x and particulate emissions while maintaining high thermal efficiency (Agarwal et al., 2017; Reitz & Duraisamy, 2015). The reduction in NO_x emissions in ACI engines compared to conventional diesel combustion (CDC) is a straightforward consequence of the lower in-cylinder temperatures in ACI (Agarwal et al., 2017). However, the dependence of the formation of particulate emissions on in-cylinder temperature is more complex. Engine emissions studies have shown that while the LTC conditions in ACI engines reduce the formation of mature soot

compared to CDC, they are conducive for the formation of POA (Lucachick et al., 2016; Moses-DeBusk et al., 2019; Northrop et al., 2011; Park et al., 2023; Storey et al., 2016). We have observed signatures of both second-stage POA (incipient soot) and first-stage POA (OxyPOA) in the emissions of a compression-ignition engine operated using an ACI strategy (premixed charge compression ignition (PCCI)) (Omar El Hajj et al., 2024).

Blendstocks with high RON (i.e. single-stage ignition) are usually added to gasoline fuel to boost the overall RON (Anderson et al., 2012). The utilization of high-RON blendstocks has also been explored as means to modulate autoignition in ACI engines. For example, a major challenge in the development of the homogeneous charge compression ignition (HCCI) engine, a prominent ACI strategy, is controlling LTHR for optimal performance at variable engine loads. HCCI engines are stable at partial loads, but are subject to premature autoignition, thus engine knock at high loads (Böğrek et al., 2021; Lü et al., 2007). Adding high RON blendstocks to diesel-like (high-reactivity) fuels has been explored as LTHR inhibitors in order to extend the operation range of HCCI engines (Böğrek et al., 2021; P. Saisirirat et al., 2011; Peerawat Saisirirat et al., 2010).

A wide variety of high-RON blendstocks have been studied in both spark-ignition and ACI engine applications. Notable examples include ethanol (Herrmann et al., 2014; P. Saisirirat et al., 2011; Saisirirat et al., 2010), 1-butanol (Saisirirat et al., 2011; Saisirirat et al., 2010), and toluene (Böğrek et al., 2021; Chen et al., 2022; Lee et al., 2019; Waqas et al., 2019). Additionally, some advanced biofuels such as dimethyl ether (DME) (Burke et al., 2015; Rodriguez et al., 2015) and furan derivatives, including 2-methylfuran (2-MF) and 2,5-dimethylfuran (DMF), have been proposed (Alexandrino, 2020; Fioroni et al., 2022; Singh et al., 2018). Recent investigations revealed that blendstocks can have non-linear effects on the overall RON of the fuel, which is dependent on the effectiveness of the blendstock at scavenging radicals formed during first-stage ignition (Singh et al., 2018). On the one hand, some blendstocks yield higher RON values than what would be expected based on a linear-blending model. This phenomenon, referred to as synergistic blending, offers a notable advantage as it allows for achieving the desired RON target with a lower volume of blendstock (Fioroni et al., 2022; Foong et al., 2014). On the other hand, some blendstocks

exhibit antagonistic blending behavior, where the blend RON is less than that predicted by a linear-blending model (Fioroni et al., 2022; Foong et al., 2014).

In this paper, we investigate the effect of high-RON blendstocks, on the formation of OxyPOA during first-stage combustion of binary blends with *n*-heptane. We consider structurally diverse blendstocks, including toluene, ethanol, and DMF in order to assess the effect of blendstock molecular structure on the *n*-heptane consumption and, consequently, OxyPOA formation. While the blendstocks do not exhibit two-stage ignition behavior and thus do not form QOOH radicals that precede cyclic ethers and OxyPOA, they influence the combustion of the binary blends due to interaction with the OH radicals generated from *n*-heptane. Furthermore, ethanol and DMF were reported to exhibit synergistic blending with *n*-heptane for RON (Christensen et al., 2011; Fioroni et al., 2022; Foong et al., 2014; Singh et al., 2018). Therefore, we specifically chose these two blendstocks to explore whether their synergistic blending for RON translates into synergistic blending for suppressing OxyPOA formation.

2. Materials and methods

2.1. Combustion experiments

We conducted experiments to investigate OxyPOA formation in the combustion of binary fuel blends with *n*-heptane as the primary fuel. We chose *n*-heptane as the primary fuel due to its high reactivity (prominent two-stage ignition behavior) and because it has been utilized as the primary fuel in recent studies that investigated the effect of blendstocks on RON (Böğrek et al., 2021; Dagaut & Togbé, 2010; Foong et al., 2014; Lü et al., 2007; Tripathi et al., 2018). We incorporated three blendstocks that have been investigated for their ability to boost RON and improve autoignition properties in ACI engines: toluene (Böğrek et al., 2021; Lee et al., 2019; Waqas et al., 2019), ethanol (Lü et al., 2007; Peerawat Saisirirat et al., 2010), and 2,5-dimethylfuran (DMF) (Alexandrino, 2020). Mixtures of *n*-heptane and each blendstock were blended on molar basis, maintaining an equivalence ratio (ϕ) of 1 and $O_2/N_2 = 0.1$. We employed blendstock molar ratios of 0% (i.e. pure *n*-heptane), 30%, 50%, and 70%. In order to capture OxyPOA formation, the

experiments were performed at combustion temperatures ranging between 500 K and 850 K, which span the first-stage ignition regime.

The experimental setup used in the combustion experiments is similar to that described in our previous works (O El Hajj et al., 2021; Omar El Hajj et al., 2024), but was modified to enable the use of binary fuel mixtures. The combustion was performed in a 0.24 L quartz reactor enclosed in an insulated heater controlled by a temperature controller (OMEGA, model CNi3244). The fuel blend was introduced into the reactor by flowing ultra-high purity N_2 into a dual-bubbler system, with the desired blending ratio set by controlling the flowrate of nitrogen in each bubbler using mass flow controllers (GC1 Series, Dakota Instruments, NY, USA). The bubbler design ensured that the N_2 exiting the bubbler was saturated with the fuel, as confirmed by mass transfer calculations (Z. Cheng et al., 2019). Therefore, the molar flowrate of each fuel could be calculated from knowledge of the fuel's saturation pressure and N_2 flowrate. The fuel blend flow was then mixed with additional N_2 and clean, dry air to obtain the desired ϕ and O_2/N_2. The total flow rate entering the reactor was set at 1 standard liter per minute (SLPM), resulting in an average residence time of 14.4 seconds.

The emissions from the reactor were diluted in a 4 L glass dilution chamber using clean, dry air prior to sampling. We continuously measured the emitted aerosol particle size distribution at 90-second resolution using a scanning mobility particle sizer (SMPS, TSI model 3882) in the range of 10-500 nm. The SMPS uses an electrostatic classifier (TSI, Model 3082), a long differential mobility analyzer (DMA, TSI, Model 3081A00), and an advanced aerosol neutralizer (TSI, Model 3088), along with a condensation particle counter (CPC, TSI, Model 3772). We obtained the total aerosol mass concentrations ($\mu g/m^3$) by integrating the size distributions using a particle density of 1.3 g/cm^3 that we previously obtained using tandem differential mobility analyzer – aerosol particle sizer (tandem DMA-APM) measurements for OxyPOA emissions from pure *n*-heptane combustion (O El Hajj et al., 2021). We assumed that the particle density is similar for OxyPOA emissions for the different blends.

2.2. Chemical kinetics simulations

Aggregated species profiles for all cyclic ether isomers of *n*-heptane (Supplementary Information (SI) Figure S1) and reaction pathway flux analyses on OH radicals were simulated at the conditions of the experiments (SI Table S1) using the perfectly stirred reactor module in the ChemKin program. The reaction mechanism of Cheng et al. (S. Cheng et al., 2021) (1,956 species, 10,295 reactions) was used for *n*-heptane and binary blends with toluene and with ethanol. Because only reduced mechanisms (Bhattacharya et al., 2021; Li et al., 2022) are reported for blends of *n*-heptane with DMF, chemical kinetics simulations were not conducted since the reduction processes necessarily employ species lumping wherein elementary reactions for relevant radicals, such as QOOH, are grouped into a single, representative step. The effect of the simplification procedure is inadequate description of isomer-specific reactions that are relevant to the formation of cyclic ethers, which are central to OxyPOA. It is important to note that the development of the Cheng et al. (S. Cheng et al., 2021) mechanism, and chemical kinetics mechanisms for combustion in general, center on chain-reaction sequences underpinning predictions of gas-phase ignition behavior of hydrocarbons and biofuels, rather than nascent particle-formation steps leading to aerosols, the chemical mechanisms for which differ substantially. Additional work is required to produce mechanisms capable of describing gas-phase ignition chemistry simultaneous with aerosol formation at combustion conditions.

2.3. Chemical speciation

We performed chemical analysis on the OxyPOA emissions using electrospray ionization Fourier-transform ion cyclotron resonance mass spectrometry (ESI-FTIRC-MS) for its efficacy at detecting the oxygenated compounds we have previously shown to constitute OxyPOA (Omar El Hajj et al., 2024). We collected aerosol samples at combustion temperatures that generated the maximum OxyPOA emissions for each of the blends (see Section 3.2). The samples were collected on 47 mm polytetrafluoroethylene (PTFE) filters with 0.2 μm pore size (Whatman, Maidstone, UK) at a flowrate of 5 SLPM. We targeted mass loadings of ~150 μg, which was estimated from the online SMPS measurements and flowrate through the filter. Solvent extracts were prepared by ultrasonic washing of the filters immersed in 2 ml of acetonitrile (≥ 99.9% purity, Fisher Scientific). Analysis was performed on a Bruker SolariX 12T FTICR mass

spectrometer (Bruker Daltonik, GmbH, Bremen, Germany) in negative ion mode. Mass spectra were collected between mass-to-charge (*m/z*) ratios from 75-800 at a flowrate of 2.0 µL/min and a capillary voltage of 4.5 kV. Calibration was performed with sodium trifluoroacetate (>97%, Sigma-Aldrich) (0.1 mg/mL in 50:50 methanol:water). Spectra were collected in triplicate by doing three injections of 10 µL per sample. The capillary was flushed with methanol to remove residual compounds between injections. Prior to introducing samples to the instrument, mass spectra of methanol and extraction blanks were acquired and subtracted from the mass spectra of the sample.

We analyzed average data obtained from 48 scans per injection for each sample using the Bruker Compass Data Analysis software (Version 5.3) and background subtraction was performed using Xpose mode with a retention time window of 0.0083s and a ratio of 5 in order to minimize noise and extraction blank signals. For features with S/N > 1, MFAssignR (Schum et al., 2020), an open source R package molecular formulas assignment for ultra-high resolution mass spectrometry, was used for component molecular assignment. Assignments were internally recalibrated and subjected to the following restrictions: CxHyOz; $0.3 \leq H/C \leq 3$; $O/C \leq 2.5$, and a maximum allowable error of 1 ppm. The final peak list used in the interpretations for each sample was composed of only molecular assignments that were common across the three injections.

3. Results

3.1. Effect of blendstocks on oxygenated primary organic aerosol (OxyPOA) formation pathways

Figure 1a shows the mass spectrum of OxyPOA emissions from the combustion of *n*-heptane, obtained using ESI-FTIRC-MS. The mass spectrum exhibits repetitive structures separated by 14 u that are indicative of oligomer formation, as we have previously observed in OxyPOA emissions from *n*-heptane and *n*-pentane combustion (Omar El Hajj et al., 2024). The 14 u separation is a consequence of dominant monomer formation pathways initiated by reactions of cyclic ethers with OH radicals that involve sequential steps of adding one oxygen atom and abstracting two hydrogen atoms (Omar El Hajj et al., 2024). As shown in Figure 1b-d, mass spectra of OxyPOA emissions from all blends exhibit features that are similar to pure *n*-heptane. This indicates that while the blendstocks reduce the available OH radical pool, the gas-phase

chemistry implicated in the formation of cyclic ethers and consequently OxyPOA monomers remain prevalent.

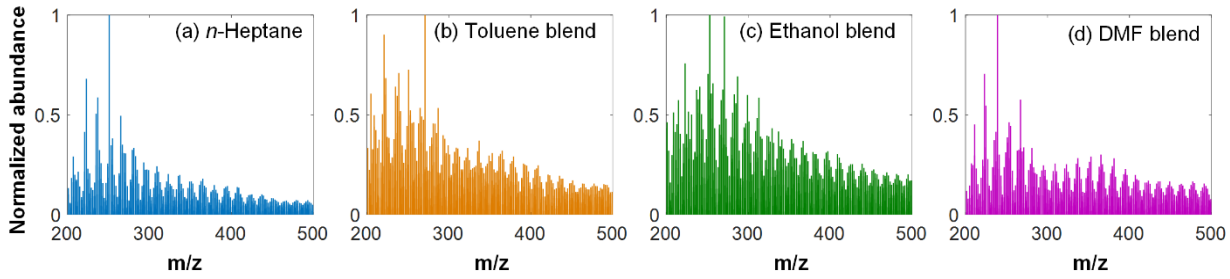

Figure 1. Mass spectra obtained using ESI-FTICR-MS of OxyPOA emitted from the combustion of (a) *n*-heptane, (b) *n*-heptane/toluene blend, (c) *n*-heptane/ethanol blend, and (d) *n*-heptane/DMF blend. For the blends, the mass spectra are for OxyPOA samples collected for blendstock molar ratio of 30% and at the combustion temperature corresponding to the peak emission for each blendstock (see Figure 4 and SI Table S2-S5). The mass spectra are shown for the *m/z* range 200 u – 500 u for clarity. The full mass spectra and corresponding molecular assignments are given in the Supplementary Material (SM).

However, the reactions of the blendstocks with OH radicals can produce species that potentially contribute to OxyPOA formation via pathways different from those associated with the cyclic ethers produced by *n*-heptane combustion. To explore the importance of these blendstock-specific OxyPOA formation pathways, Figure 2 depicts van Krevelen plots of OxyPOA produced from the combustion of *n*-heptane and the different blendstocks and Figure 3 depicts classification of the molecular assignments based on the modified aromaticity index (AI_{mod}) (B.P. Koch, 2015; Koch Dittmar, T., 2006). Following the approach of Vandergrift et al. (Vandergrift et al., 2022), we applied the AI_{mod} framework to classify the molecular formulas into aliphatic ($AI_{mod} < 0$), low O unsaturated ($0 < AI_{mod} \leq 0.5$ and $O/C < 0.5$) , high O unsaturated ($0 < AI_{mod} \leq 0.5$ and $O/C \geq 0.5$), and aromatic ($AI_{mod} > 0.5$).

As shown in Figure 3, 12% of the OxyPOA molecules emitted by *n*-heptane combustion are classified as aromatic. Even though the temperatures during first-stage ignition are not high enough to produce conventional aromatic structures (e.g. polycyclic aromatic hydrocarbons), they produce oxidized cyclic ethers that form the building blocks for OxyPOA (Omar El Hajj et al., 2024) and are classified as aromatic, though of lower aromaticity than benzene (Fringuelli et al., 1974). For example, the molecular formula $C_7H_6O_5$ (coincides with *m/z* 169.014 detected in the OxyPOA mass spectra in all experiments) that

potentially corresponds to a highly oxidized cyclic ether produced in first-stage *n*-heptane combustion has AI_{mod} = 0.6 and is classified as aromatic.

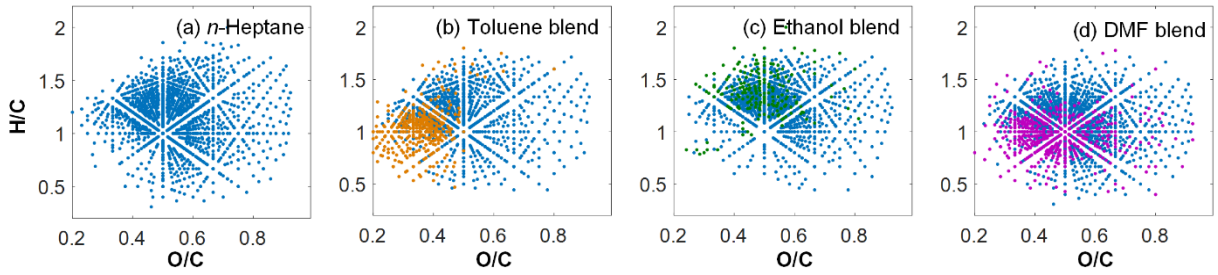

Figure 2. van Krevelen plots of the molecular assignments of OxyPOA emitted from the combustion of (a) *n*-heptane, (b) *n*-heptane/toluene blend, (c) *n*-heptane/ethanol blend, and (d) *n*-heptane/DMF blend. For the blends, the molecular assignments are for OxyPOA samples collected for blendstock molar ratio of 30% and at the combustion temperature corresponding to the peak emission for each blendstock (see SM Table S2-S5). For panels (b)-(d), the blue dots correspond to molecular assignments common with *n*-heptane and the dots with other colors correspond to molecular assignments unique to the blend (i.e. not observed in *n*-heptane).

For the blends, we apportioned the molecular formulas into those common with *n*-heptane (i.e. molecular assignments observed in the mass spectra of both *n*-heptane and the blend) and those unique to the blend (i.e. molecular assignments observed in the mass spectrum of the blend but not *n*-heptane). The fractions of unique molecular formulas for DMF blend (30%) and toluene blend (29%) are similar and significantly larger than the ethanol blend (16%). This finding suggests that the propensity to produce OxyPOA is similar for the reactions of DMF and toluene with OH, but significantly smaller for ethanol. We note that the propensity to produce OxyPOA is a function of not only the rate of the reaction with OH, but also the yields of condensable species (i.e. species that have low-enough volatility to partition to the particle phase). OA formation from the reactions of aromatic species (including toluene) with OH has not been previously investigated in LTC, but has been extensively studied in the context of secondary organic aerosol (SOA) formation in the atmosphere (Seinfeld & Pandis, 2016). More recently, furans (including DMF) have also been recognized as important SOA precursors in the atmosphere (El Mais et al., 2023).

As shown in Figure 2b, the molecular formulas unique to the toluene blend cluster in the low O/C region of the van Krevelen plot, indicating distinct OxyPOA formation pathways associated with toluene oxidation that involve less oxygen addition compared to the cyclic ethers produced by *n*-heptane combustion.

However, the molecular formulas unique to the DMF blend (Figure 2d), though skewed more toward the low O/C region, exhibit more overlap with the molecules that are common with *n*-heptane. Given the similar molecular structure of DMF and the cyclic ethers produced in *n*-heptane combustion, it is possible that the production of OxyPOA from DMF oxidation follows similar pathways to those of the cyclic ethers in that a peroxy radical of DMF may undergo bimolecular reaction to form an aromatic ROOH, which may lead to 5-methylfuran-2-carbaldehyde ($C_6H_6O_2$). A similar process could repeat to form furan-2,5-dicarbaldehyde ($C_6H_4O_3$).

The unique molecular formulas in both the toluene blend and DMF blend have significantly higher fractions of aromatics compared to *n*-heptane (Figure 3). Both toluene (C_7H_8; AI_{mod} = 0.57) and DMF (C_6H_8O; AI_{mod} = 0.45) are significantly more unsaturated than the cyclic ethers produced in *n*-heptane combustion ($C_7H_{14}O$; AI_{mod} = 0.08). Consequently, the toluene and DMF reactions with OH are more conducive for producing molecules with AI_{mod} > 0.5 than the cyclic ether produced by *n*-heptane, which would explain the larger fraction of molecular formulas classified as aromatic in the toluene blend and DMF blend compared to *n*-heptane.

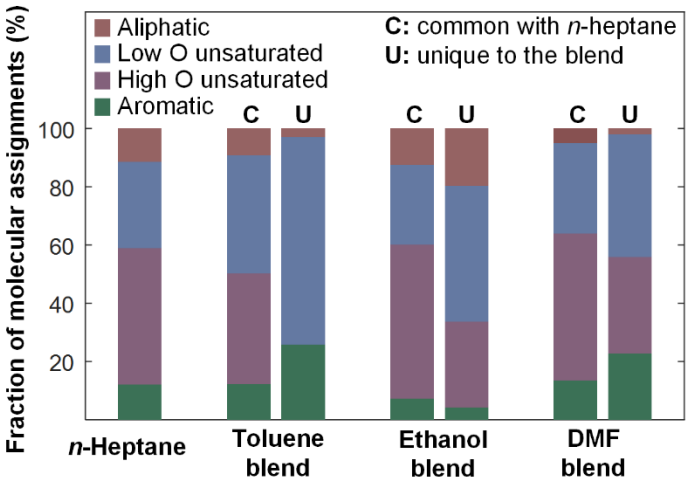

Figure 3. Modified aromaticity index (AI_{mod}) classification of the molecular assignments of OxyPOA emitted from the combustion of (a) *n*-heptane, (b) *n*-heptane/toluene blend, (c) *n*-heptane/ethanol blend, and (d) *n*-heptane/DMF blend. For the blends, the molecular assignments are for OxyPOA samples collected for blendstock molar ratio of 30% and at the combustion temperature corresponding to the peak emission for each blendstock (see SI Table S2-S5).

The reaction of ethanol with OH does not produce appreciable yields of condensable species. However, the major product of R + O_2 reactions, where R is hydroxy-ethyl, is acetaldehyde (da Silva et al., 2009), which may yield glyoxal (Suarez-Bertoa et al., 2015). Such aldehydes do not have low-enough volatility to condense and form OxyPOA, but can exhibit uptake to water in the particles and form hydrates that consequently form oligomers (Corrigan et al., 2008; Hastings et al., 2005), and have been shown to contribute to SOA formation (Suarez-Bertoa et al., 2015). OxyPOA produced from *n*-heptane combustion has relatively high O/C, where the majority of the molecules shown in Figure 2 have O/C > 0.3 and fall within the oxygenated OA (OOA) range. High O/C is indicative of increased hygroscopicity (Jimenez et al., 2009), thus OxyPOA is expected to adsorb water vapor emitted from the combustion reaction, providing sites for aldehydes uptake. The molecules attributed to aldehyde hydrates within the OxyPOA matrix would explain the relatively high H/C ratios of the unique molecules in the ethanol blend (Figure 2c and Table S6) and high abundance of molecules classified as aliphatic compared to the toluene blend and the DMF blend (Figure 3).

3.2. Effect of blendstocks on oxygenated primary organic aerosol (OxyPOA) emission profiles

Figure 4 shows the mass concentrations of OxyPOA emissions at different combustion temperatures for *n*-heptane and *n*-heptane blended with the different blendstocks. In concordance with our previous results (O El Hajj et al., 2021), *n*-heptane combustion emitted OxyPOA within the temperature range of 500 K – 700 K, with peak emissions around 560 K. This OxyPOA emission profile coincides with first-stage ignition, as confirmed by the fuel-depletion profiles obtained using ChemKin simulations of gas-phase reactions (Figure 5 and Figure 6). As shown in Figure 4, the addition of blendstocks led to a shift in OxyPOA emission profiles to higher temperatures and overall reduction in the peak emissions. For both the ethanol blend and DMF blend, the OxyPOA concentrations were reduced below the detection limit at blendstock molar ratio of 70%. These results are in-line with the effect of blendstocks on fuel reactivity, as confirmed by the ChemKin simulations illustrated in Figure 5 and Figure 6, and are a consequence of the reduction in the available OH radical pool required for OxyPOA formation. We ascribe the reduction in OH radicals to two reasons: (i) the molar displacement of *n*-heptane with the blendstock reduces the production of OH radicals

during the first-stage ignition of *n*-heptane; and (ii) the blendstocks react with OH at rates similar to that of *n*-heptane (Sivaramakrishnan & Michael, 2009; Stranic et al., 2014; Vasudevan et al., 2005; Whelan et al., 2020) and favor chain-terminating reactions that do not lead to regeneration of OH. Consequently, all three blendstocks act as sinks for OH radicals generated from *n*-heptane that otherwise foster chain-branching. Subsequent reactions of OH radicals with toluene, ethanol, and DMF do not contribute to the production of cyclic ethers due to the lack of necessary chemical pathways, namely ROO → QOOH → cyclic ether + OH (Rotavera & Taatjes, 2021).

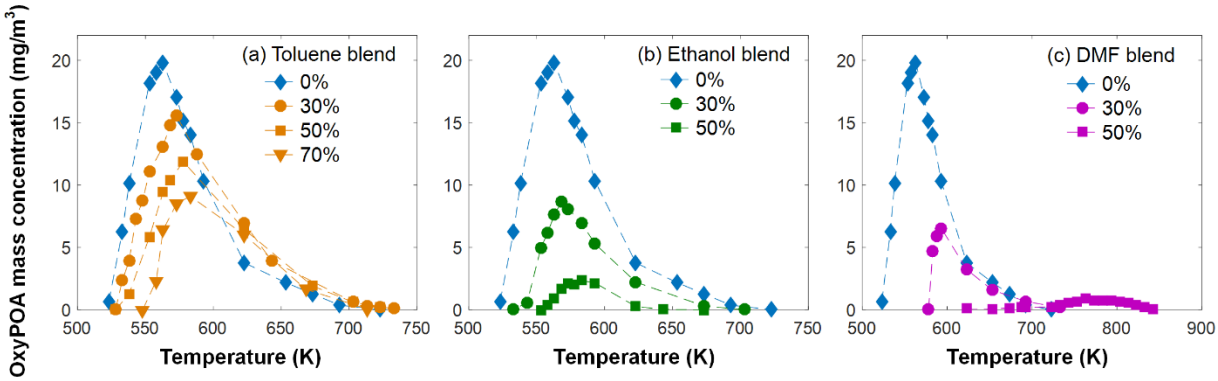

Figure 4. Mass concentration of OxyPOA emitted from the combustion of (a) *n*-heptane/toluene blend, (b) *n*-heptane/ethanol blend, and (c) *n*-heptane/DMF blend. The % values correspond to the molar ratio of the blendstock (0% corresponds to pure *n*-heptane). The mass concentrations were below the detection limit at molar ratio of 70% for the *n*-heptane/ethanol blend and *n*-heptane/DMF blend. Each data point is the average of 5 measurements. The standard deviations are smaller than the symbol size and are not shown in the figure. Numerical values (averages and standard deviations) are given in SI Table S2-S5.

Figure 5a shows depletion profiles for *n*-heptane and the binary blends with toluene. The trend for each case exhibits NTC behavior starting near 600 K, which is due to a shift in the balance of reactions derived from RO_2 away from chain-branching and toward chain-propagating and chain-inhibiting. The simulations also show the lower depletion rates of *n*-heptane with increasing toluene molar ratio in the blend. Figure 5b shows the corresponding trends in concentration for the sum of all *n*-heptane-derived cyclic ethers. The reduction in cyclic ether yield in the blends is due to the consumption of OH radicals by toluene, which are produced via QOOH + O_2 (step *iv* in Figure 5c), leading to one OH radical (step *v*) and a ketohydroperoxide, which subsequently yields two additional radicals (step *vi*) from unimolecular decomposition into OH +

carbonyl-oxy radical. Reaction pathway analysis was conducted at 600 K and 700 K to determine the effect of blend composition on OH formation and consumption pathways. For both temperatures, H-abstraction reactions yielding the four distinct carbon-centered radicals of *n*-heptane were the major sinks of OH, yet similar reactions with toluene yielding benzyl + H_2O were competitive on a site-specific basis.

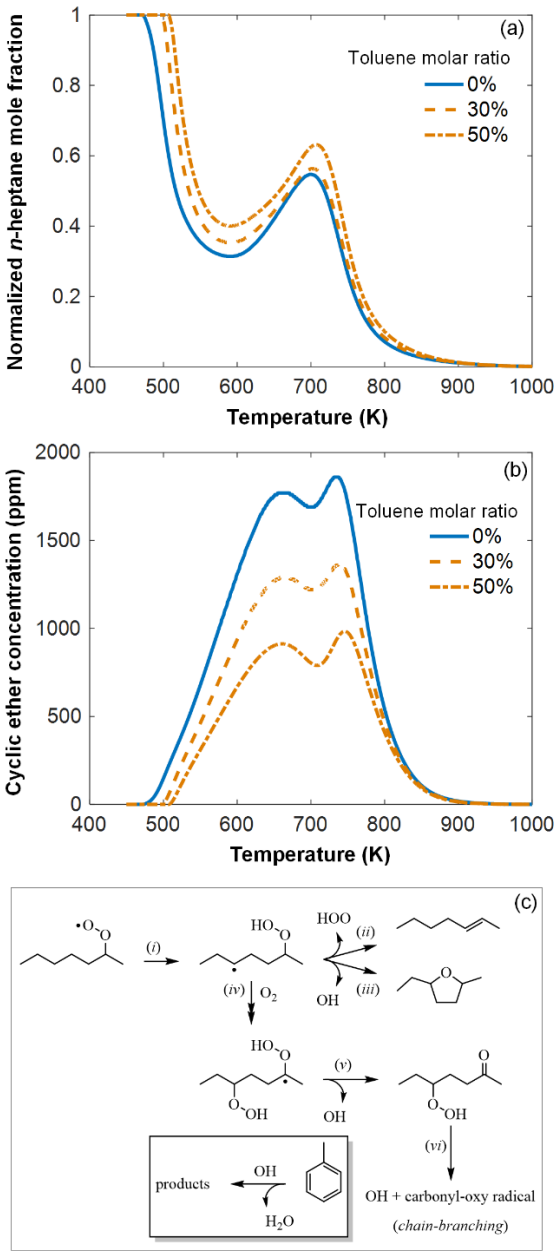

Figure 5. Species profiles of (a) *n*-heptane and (b) the sum of *n*-heptane-derived cyclic ethers for the *n*-heptane/toluene blend. (c) Low-temperature oxidation for a representative RO_2 species of *n*-heptane, 2-heptylperoxy, which follows a degenerate chain-branching mechanism that increases OH generation via pathway (*iv*). In the presence of toluene, a portion of the OH radicals produced from *n*-heptane is consumed, thus suppressing the formation of cyclic ethers and consequently OxyPOA.

Similar results were produced for the blends of ethanol with *n*-heptane. Figure 6a shows depletion profiles for *n*-heptane and the two binary blends with ethanol. The simulations also show the lower depletion rates of *n*-heptane with increasing ethanol concentration in the blend for the same reasons observed in the toluene blends. Figure 6b shows the corresponding trends in concentration for the sum of all *n*-heptane-derived cyclic ethers. The reduction in yield with each blend is due to some of the OH radicals produced from *n*-heptane via QOOH-mediated reactions being consumed by ethanol rather than initiating a heptyl radical. As with toluene, reaction of OH with ethanol yields species that do not contribute to cyclic ethers. Instead, acetaldehyde is the primary product of ethanol (Figure 6c). Reaction pathway analysis was conducted at 600 K and 700 K to determine the effect of blend composition on OH formation and consumption pathways. For both temperatures, H-abstraction reactions yielding the four distinct carbon-centered radicals of *n*-heptane remained the major sinks of OH, as with toluene. Reactions of OH to form both of the carbon-centered radicals of ethanol were competitive on a site-specific basis.

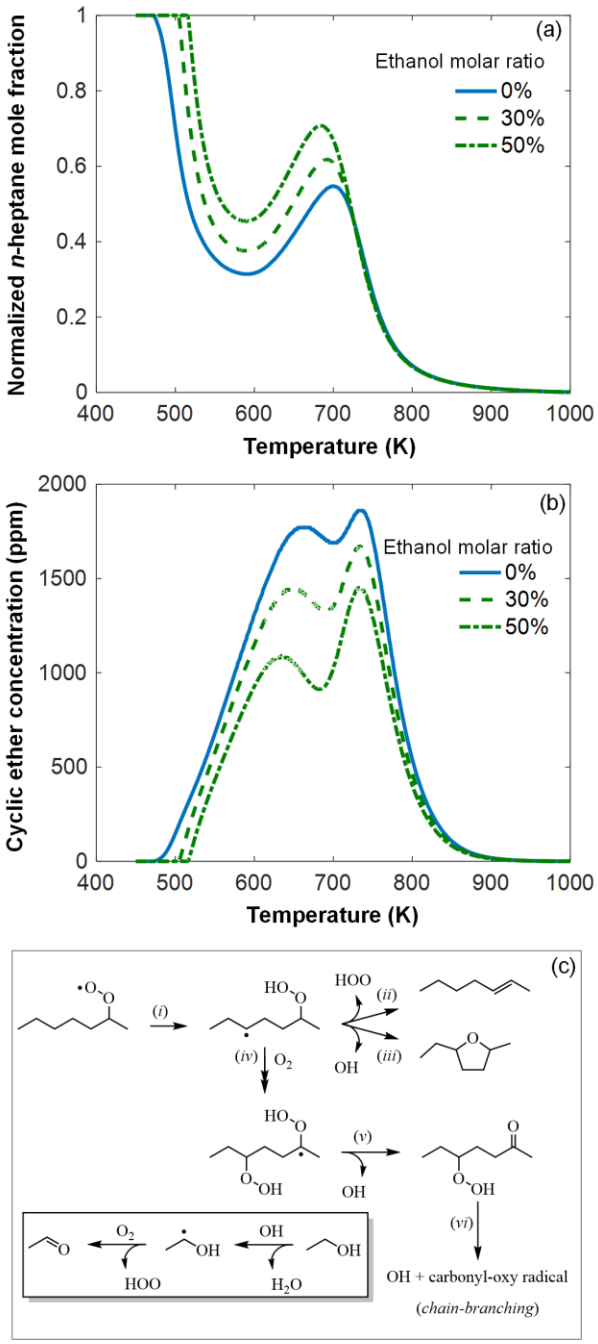

Figure 6. Species profiles of (a) *n*-heptane and (b) the sum of *n*-heptane-derived cyclic ethers for the *n*-heptane/ethanol blend. (c) Low-temperature oxidation for a representative RO_2 species of *n*-heptane, 2-heptylperoxy, which follows a degenerate chain-branching mechanism that increases OH generation via pathway (*iv*). In the presence of ethanol, a portion of the OH radicals produced from *n*-heptane are consumed to form hydroxyethyl radicals, which upon reaction with O_2 predominantly yield acetaldehyde + HOO. The net effect is suppressing the formation of cyclic ethers and consequently OxyPOA.

The peak OxyPOA mass concentrations from all experiments in Figure 4 are plotted versus blendstock molar ratio in Figure 7. The dashed line in Figure 7 represents a hypothetical linear reduction in OxyPOA

mass concentrations due to molar displacement of *n*-heptane by the blendstock, which is analogous to the linear blending model that calculates the RON of the blend as the average of the RON of the primary fuel and that of the blendstock (Fioroni et al., 2022). Based on this framework, we categorize blends emitting OxyPOA mass concentrations below the linear reduction as synergistic for OxyPOA suppression and those emitting OxyPOA mass concentrations above the linear reduction as antagonistic for OxyPOA suppression. As described above, blendstocks suppress OxyPOA emissions by suppressing chain-branching/second-O_2-addition associated with the *n*-heptane reactivity due to inhibiting the formation of OH radicals by molar displacement of *n*-heptane as well as scavenging OH radicals. However, beyond suppressing *n*-heptane reactivity, there are two additional effects that are specific to OxyPOA formation. First, the reaction of the blendstock with OH can itself produce OxyPOA, as described in Section 3.1. Second, OxyPOA formation involves gas-particle partitioning of intermediate-volatility and semi-volatile species as well as oligomer formation in the particle phase (Omar El Hajj et al., 2024). Both of these phenomena are governed by thermodynamic equilibrium (Donahue et al., 2006; Trump & Donahue, 2014) and depend on the concentration of condensable species produced via gas-phase chemistry. Reduction in the concentration of the condensable species shifts the gas-particle equilibrium partitioning to the gas phase leading to super-linear reduction in OxyPOA. Furthermore, the reduction in condensed OxyPOA monomers leads to less oligomer formation and further reduction in OxyPOA.

To summarize, the extent of OxyPOA suppression associated with blendstocks is a result of interplay between (i) molar displacement of the high-reactivity primary fuel, (ii) inhibiting chain propagation reactions by scavenging OH radicals, (iii) production of OxyPOA from the reaction of blendstocks with OH radicals, and (iv) shifting the gas-particle thermodynamic equilibrium toward the gas phase. The first two effects are common with the effect of blending on RON (Fioroni et al., 2022), while the last two effects are specific to OxyPOA formation.

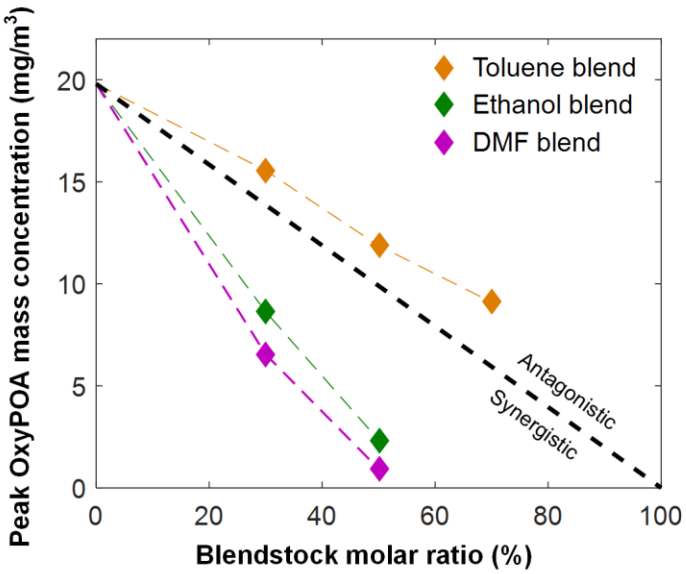

Figure 7. Peak mass concentration of OxyPOA emitted from the combustion of *n*-heptane/toluene blend, *n*-heptane/ethanol blend, and *n*-heptane/DMF blend for different blendstock molar ratios. The dashed black line corresponds to hypothetical linear reduction in OxyPOA mass concentrations due to molar displacement of *n*-heptane by the blendstock. The standard deviations are smaller than the symbol size and are not shown in the figure. Numerical values (averages and standard deviations) are given in SI Table S2-S5.

As shown in Figure 7, toluene exhibited antagonistic blending for OxyPOA suppression. This result is consistent with the relatively high yield of OxyPOA produced from the reaction, as described in Section 3.1. Both ethanol and DMF exhibited synergistic blending for OxyPOA suppression, coincident with their reported synergistic blending for RON due to their ability to efficiently reduce the OH radical pool (Christensen et al., 2011; Fioroni et al., 2022; Foong et al., 2014; Singh et al., 2018). Even though DMF reaction with OH radicals produced a significantly higher yield of OxyPOA compared to ethanol (Section 3.1), its synergistic blending for OxyPOA suppression was more prominent. This result indicates that the ability of DMF to scavenge OH radicals, leading to its superior RON boosting compared to ethanol (Fioroni et al., 2022) (effect (ii) listed above), is more dominant than the additional OxyPOA formation from its reaction with OH radicals (effect (iii) listed above).

4. Discussion and conclusions

Previous studies have demonstrated that the reactivity of two-stage ignition fuels can be modulated by introducing high-RON blendstocks that can exhibit either synergistic or antagonistic blending, depending on their ability to scavenge OH radicals that form during first-stage ignition (Fioroni et al., 2022; Foong et al., 2014). Here, we show that the shift to higher temperatures, and overall reduction in fuel reactivity and formation of cyclic ethers predicted by chemical kinetics simulations (Figure 5 and Figure 6) are reflected in OxyPOA formation profiles obtained from the experiments (Figure 4). Furthermore, the synergistic and antagonistic blending for RON reported by previous studies is also reflected in suppression of OxyPOA formation. Adding all blendstocks considered in this study (toluene, ethanol, DMF) to *n*-heptane led to suppression of OxyPOA compared to pure *n*-heptane. The reduction in OxyPOA in the toluene blend was less than what is calculated from molar displacement of *n*-heptane, which can be considered as antagonistic blending for OxyPOA suppression. The reduction in OxyPOA in the ethanol blend and DMF blend was more than what is calculated from molar displacement of *n*-heptane, which can be considered as synergistic blending for OxyPOA suppression. DMF exhibited more synergistic blending for OxyPOA suppression compared to ethanol, which is consistent with its superior synergistic blending for RON (Fioroni et al., 2022). DMF is an advanced drop-in biofuel with high RON that has been extensively studied for implementation in internal combustion engines (Qian et al., 2015; Rothamer & Jennings, 2012; Somers et al., 2013). Our findings indicate that incorporating DMF has the added benefit of suppressing the formation of aerosol pollution.

In our previous works (O El Hajj et al., 2021; Omar El Hajj et al., 2024), we reported the formation of first-stage POA (OxyPOA) during low-temperature combustion of high-reactivity hydrocarbon fuels, which have formation pathways and chemical composition that are distinct from traditional POA. We showed that OxyPOA resembles SOA in that it is comprised of highly oxygenated molecules and its formation involves oligomerization in the particle phase. In this study, we demonstrate that low-reactivity (high-RON) blendstocks, which do not undergo combustion in the first-stage ignition temperature range (500 K – 700 K), can react with the OH radicals generated during first-stage ignition of the high-reactivity fuel and

produce POA. The formation pathways of this "blendstock first-stage POA" are different from the OxyPOA produced from the high-reactivity fuel that involve sequential oxidation reactions of cyclic ethers (Omar El Hajj et al., 2024). However, the blendstock first-stage POA is (i) also more oxygenated compared to traditional POA and (ii) forms in the same temperature range as OxyPOA. Therefore, for practicality, the blendstock first-stage POA can be subsumed under OxyPOA.

The blendstocks considered in this study (toluene, ethanol, DMF) react with OH radicals in the atmosphere and produce SOA. Here, we demonstrate that the blendstocks undergo similar reactions with OH radicals in LTC and produce OxyPOA. This finding further confirms our previous report (Omar El Hajj et al., 2024) that OxyPOA emitted from internal combustion engines, especially at cold-start conditions, has a similar chemical composition to SOA and can be misattributed to SOA in atmospheric measurements. Furthermore, our findings highlight the importance of improving chemical kinetics models for hydrocarbons and biofuels for not only understanding low-temperature combustion chemistry, but also pollution formation behavior.

Acknowledgments

ESI- FTICR-MS measurements were performed at the University of Georgia Proteomics and Mass Spectrometry Core Facility.

Funding

This work was supported by the National Science Foundation, Division of Chemical, Bioengineering, Environmental, and Transport Systems (CBET-2125064). FTICR was purchased with funding from the National Institutes of Health under grant NIH-S10-OD025118.

References

Agarwal, A. K., Singh, A. P., & Maurya, R. K. (2017). Evolution, challenges and path forward for low temperature combustion engines. *Progress in Energy and Combustion Science*, *61*, 1–56. https://doi.org/https://doi.org/10.1016/j.pecs.2017.02.001

Alexandrino, K. (2020). Comprehensive Review of the Impact of 2,5-Dimethylfuran and 2-Methylfuran on Soot Emissions: Experiments in Diesel Engines and at Laboratory-Scale. *Energy & Fuels*, *34*(6), 6598–6623. https://doi.org/10.1021/acs.energyfuels.0c00492

Anderson, J. E., DiCicco, D. M., Ginder, J. M., Kramer, U., Leone, T. G., Raney-Pablo, H. E., & Wallington, T. J. (2012). High octane number ethanol–gasoline blends: Quantifying the potential benefits in the United States. *Fuel*, *97*, 585–594. https://doi.org/https://doi.org/10.1016/j.fuel.2012.03.017

B.P. Koch, T. D. (2015). From mass to structure: an aromaticity index for high-resolution mass data of natural organic matter. *Rapid Communications in Mass Spectrometry*, *30*(1), 250. https://doi.org/https://doi.org/10.1002/rcm.7433

Bhattacharya, A., Shahanaghi, A., Kaario, O., Vuorinen, V., Tripathi, R., & Sarjovaara, T. (2021). Effects of blending 2,5-dimethylfuran and dimethyl ether to toluene primary reference fuels: A chemical kinetic study. *Fuel*, *304*, 121401. https://doi.org/https://doi.org/10.1016/j.fuel.2021.121401

Böğrek, A., Haşimoğlu, C., Calam, A., & Aydoğan, B. (2021). Effects of n-heptane/toluene/ethanol ternary fuel blends on combustion, operating range and emissions in premixed low temperature combustion. *Fuel*, *295*, 120628. https://doi.org/https://doi.org/10.1016/j.fuel.2021.120628

Burke, U., Somers, K. P., O'Toole, P., Zinner, C. M., Marquet, N., Bourque, G., et al. (2015). An ignition delay and kinetic modeling study of methane, dimethyl ether, and their mixtures at high pressures. *Combustion and Flame*, *162*(2), 315–330. https://doi.org/https://doi.org/10.1016/j.combustflame.2014.08.014

Chen, B., Liu, P., Xu, Q., Wang, Z., Roberts, W. L., & Pitsch, H. (2022). Low temperature oxidation of toluene in an n-heptane/toluene mixture. *Combustion and Flame*, *242*, 112200. https://doi.org/https://doi.org/10.1016/j.combustflame.2022.112200

Cheng, S., Saggese, C., Kang, D., Goldsborough, S. S., Wagnon, S. W., Kukkadapu, G., et al. (2021). Autoignition and preliminary heat release of gasoline surrogates and their blends with ethanol at engine-relevant conditions: Experiments and comprehensive kinetic modeling. *Combustion and Flame*, *228*, 57–77. https://doi.org/https://doi.org/10.1016/j.combustflame.2021.01.033

Cheng, Z., Atwi, K., Onyima, T., & Saleh, R. (2019). Investigating the dependence of light-absorption properties of combustion carbonaceous aerosols on combustion conditions. *Aerosol Science and Technology*, 1–16. https://doi.org/10.1080/02786826.2019.1566593

Christensen, E., Yanowitz, J., Ratcliff, M., & McCormick, R. L. (2011). Renewable Oxygenate Blending Effects on Gasoline Properties. *Energy & Fuels*, *25*(10), 4723–4733. https://doi.org/10.1021/ef2010089

Corrigan, A. L., Hanley, S. W., & De Haan, D. O. (2008). Uptake of Glyoxal by Organic and Inorganic Aerosol. *Environmental Science & Technology*, *42*(12), 4428–4433. https://doi.org/10.1021/es7032394

Dagaut, P., & Togbé, C. (2010). Experimental and modeling study of the kinetics of oxidation of ethanol-n-heptane mixtures in a jet-stirred reactor. *Fuel*, *89*(2), 280–286. https://doi.org/https://doi.org/10.1016/j.fuel.2009.06.035

Donahue, N. M., Robinson, a L., Stanier, C. O., & Pandis, S. N. (2006). Coupled partitioning, dilution, and chemical aging of semivolatile organics. *Environmental Science & Technology*, *40*(8), 2635–43. Retrieved from http://www.ncbi.nlm.nih.gov/pubmed/16683603

Fioroni, G. M., Rahimi, M. J., Westbrook, C. K., Wagnon, S. W., Pitz, W. J., Kim, S., & McCormick, R. L. (2022). Chemical kinetic basis of synergistic blending for research octane number. *Fuel*, *307*,

121865. https://doi.org/https://doi.org/10.1016/j.fuel.2021.121865

Foong, T. M., Morganti, K. J., Brear, M. J., da Silva, G., Yang, Y., & Dryer, F. L. (2014). The octane numbers of ethanol blended with gasoline and its surrogates. *Fuel*, *115*, 727–739. https://doi.org/https://doi.org/10.1016/j.fuel.2013.07.105

Fringuelli, F., Marino, G., Taticchi, A., & Grandolini, G. (1974). A comparative study of the aromatic character of furan, thiophen, selenophen, and tellurophen. *Journal of the Chemical Society, Perkin Transactions 2*, (4), 332–337. https://doi.org/10.1039/P29740000332

El Hajj, O, Atwi, K., Cheng, Z., Koritzke, A. L., Christianson, M. G., Dewey, N. S., et al. (2021). Two-stage aerosol formation in low-temperature combustion. *Fuel*, *304*, 121322. https://doi.org/https://doi.org/10.1016/j.fuel.2021.121322

El Hajj, Omar, Hartness, S. W., Vandergrift, G. W., Park, Y., Glenn, C. K., Anosike, A., et al. (2024). Alkylperoxy radicals are responsible for the formation of oxygenated primary organic aerosol. *Science Advances*, *9*(46), eadj2832. https://doi.org/10.1126/sciadv.adj2832

Hastings, W. P., Koehler, C. A., Bailey, E. L., & De Haan, D. O. (2005). Secondary Organic Aerosol Formation by Glyoxal Hydration and Oligomer Formation: Humidity Effects and Equilibrium Shifts during Analysis. *Environmental Science & Technology*, *39*(22), 8728–8735. https://doi.org/10.1021/es0504461

Herrmann, F., Jochim, B., Oßwald, P., Cai, L., Pitsch, H., & Kohse-Höinghaus, K. (2014). Experimental and numerical low-temperature oxidation study of ethanol and dimethyl ether. *Combustion and Flame*, *161*(2), 384–397. https://doi.org/https://doi.org/10.1016/j.combustflame.2013.09.014

Jimenez, J. L., Canagaratna, M. R., Donahue, N. M., Prevot, A. S. H., Zhang, Q., Kroll, J. H., et al. (2009). Evolution of Organic Aerosols in the Atmosphere. *Science*, *326*(5959), 1525–1529. https://doi.org/10.1126/science.1180353

Johansson, K. O., Head-Gordon, M. P., Schrader, P. E., Wilson, K. R., & Michelsen, H. A. (2018).

Resonance-stabilized hydrocarbon-radical chain reactions may explain soot inception and growth. *Science*, *361*(6406), 997. Retrieved from http://science.sciencemag.org/content/361/6406/997.abstract

Ju, Y. (2021). Understanding cool flames and warm flames. *Proceedings of the Combustion Institute*, *38*(1), 83–119. https://doi.org/https://doi.org/10.1016/j.proci.2020.09.019

Koch Dittmar, T., B. P. (2006). From mass to structure: an aromaticity index for high-resolution mass data of natural organic matter. *Rapid Communications in Mass Spectrometry*, *20*. https://doi.org/10.1002/rcm.2386

Lee, C., Wu, Y., Wu, H., Shi, Z., Zhang, L., & Liu, F. (2019). The experimental investigation on the impact of toluene addition on low-temperature ignition characteristics of diesel spray. *Fuel*, *254*, 115580. https://doi.org/https://doi.org/10.1016/j.fuel.2019.05.163

Leone, T. G., Anderson, J. E., Davis, R. S., Iqbal, A., Reese, R. A. I. I., Shelby, M. H., & Studzinski, W. M. (2015). The Effect of Compression Ratio, Fuel Octane Rating, and Ethanol Content on Spark-Ignition Engine Efficiency. *Environmental Science & Technology*, *49*(18), 10778–10789. https://doi.org/10.1021/acs.est.5b01420

Li, S., Gao, J., Huang, C., Wei, M., Zhang, T., & Liu, J. (2022). Development of a reduced n-heptane/toluene/unsaturated furans-PAH reaction mechanism for dual-fuel engine applications. *Fuel*, *317*, 123466. https://doi.org/https://doi.org/10.1016/j.fuel.2022.123466

Lü, X., Ji, L., Zu, L., Hou, Y., Huang, C., & Huang, Z. (2007). Experimental study and chemical analysis of n-heptane homogeneous charge compression ignition combustion with port injection of reaction inhibitors. *Combustion and Flame*, *149*(3), 261–270. https://doi.org/https://doi.org/10.1016/j.combustflame.2007.01.002

Lucachick, G., Curran, S., Storey, J., Prikhodko, V., & Northrop, W. F. (2016). Volatility characterization of nanoparticles from single and dual-fuel low temperature combustion in compression ignition

engines. *Aerosol Science and Technology*, *50*(5), 436–447. https://doi.org/10.1080/02786826.2016.1163320

El Mais, A. E. R., D'Anna, B., Drinovec, L., Lambe, A. T., Peng, Z., Petit, J.-E., et al. (2023). Insights into secondary organic aerosol formation from the day- and nighttime oxidation of polycyclic aromatic hydrocarbons and furans in an oxidation flow reactor. *Atmospheric Chemistry and Physics*, *23*(23), 15077–15096. https://doi.org/10.5194/acp-23-15077-2023

Michelsen, H. A. (2017). Probing soot formation , chemical and physical evolution , and oxidation : A review of in situ diagnostic techniques and needs. *Proceedings of the Combustion Institute*, *36*(1), 717–735. https://doi.org/10.1016/j.proci.2016.08.027

Moses-DeBusk, M., Curran, S. J., Lewis, S. A., Connatser, R. M., & Storey, J. M. E. (2019). Impacts of Air-Fuel Stratification in ACI Combustion on Particulate Matter and Gaseous Emissions. *Emission Control Science and Technology*. https://doi.org/10.1007/s40825-019-00122-5

Northrop, W. F., Madathil, P. V, Bohac, S. V, & Assanis, D. N. (2011). Condensational Growth of Particulate Matter from Partially Premixed Low Temperature Combustion of Biodiesel in a Compression Ignition Engine. *Aerosol Science and Technology*, *45*(1), 26–36. https://doi.org/10.1080/02786826.2010.517579

Park, Y., Moses-DeBusk, M., Sluder, S. S., & Huff, S. P. (2023). Impact of Biofuel Blending on Hydrocarbon Speciation and Particulate Matter from a Medium-Duty Multimode Combustion Strategy. *Energies*. https://doi.org/10.3390/en16155735

Qian, Y., Zhu, L., Wang, Y., & Lu, X. (2015). Recent progress in the development of biofuel 2,5-dimethylfuran. *Renewable and Sustainable Energy Reviews*, *41*, 633–646. https://doi.org/https://doi.org/10.1016/j.rser.2014.08.085

Reitz, R. D., & Duraisamy, G. (2015). Review of high efficiency and clean reactivity controlled compression ignition (RCCI) combustion in internal combustion engines. *Progress in Energy and*

Combustion Science, *46*, 12–71. https://doi.org/https://doi.org/10.1016/j.pecs.2014.05.003

Ribaucour, M., Minetti, R., Sochet, L. R., Curran, H. J., Pitz, W. J., & Westbrook, C. K. (2000). Ignition of isomers of pentane: An experimental and kinetic modeling study. *Proceedings of the Combustion Institute*, *28*(2), 1671–1678. https://doi.org/https://doi.org/10.1016/S0082-0784(00)80566-4

Rodriguez, A., Frottier, O., Herbinet, O., Fournet, R., Bounaceur, R., Fittschen, C., & Battin-Leclerc, F. (2015). Experimental and Modeling Investigation of the Low-Temperature Oxidation of Dimethyl Ether. *The Journal of Physical Chemistry A*, *119*(28), 7905–7923. https://doi.org/10.1021/acs.jpca.5b01939

Rotavera, B., & Taatjes, C. A. (2021). Influence of functional groups on low-temperature combustion chemistry of biofuels. *Progress in Energy and Combustion Science*, *86*, 100925. https://doi.org/https://doi.org/10.1016/j.pecs.2021.100925

Rothamer, D. A., & Jennings, J. H. (2012). Study of the knocking propensity of 2,5-dimethylfuran–gasoline and ethanol–gasoline blends. *Fuel*, *98*(0), 203–212. https://doi.org/http://dx.doi.org/10.1016/j.fuel.2012.03.049

Russo, C., Tregrossi, A., & Ciajolo, A. (2015). Dehydrogenation and growth of soot in premixed flames. *Proceedings of the Combustion Institute*, *35*(2), 1803–1809. https://doi.org/https://doi.org/10.1016/j.proci.2014.05.024

Saisirirat, P., Togbé, C., Chanchaona, S., Foucher, F., Mounaim-Rousselle, C., & Dagaut, P. (2011). Auto-ignition and combustion characteristics in HCCI and JSR using 1-butanol/n-heptane and ethanol/n-heptane blends. *Proceedings of the Combustion Institute*, *33*(2), 3007–3014. https://doi.org/https://doi.org/10.1016/j.proci.2010.07.016

Saisirirat, Peerawat, Foucher, F., Chanchaona, S., & Mounaïm-Rousselle, C. (2010). Spectroscopic Measurements of Low-Temperature Heat Release for Homogeneous Combustion Compression Ignition (HCCI) n-Heptane/Alcohol Mixture Combustion. *Energy & Fuels*, *24*(10), 5404–5409.

https://doi.org/10.1021/ef100938u

Schum, S. K., Brown, L. E., & Mazzoleni, L. R. (2020). MFAssignR: Molecular formula assignment software for ultrahigh resolution mass spectrometry analysis of environmental complex mixtures. *Environmental Research*, *191*, 110114. https://doi.org/https://doi.org/10.1016/j.envres.2020.110114

Seinfeld, J. H., & Pandis, S. N. (2016). *Atmospheric Chemistry and Physics: from air pollution to climate change* (3rd ed.). Hoboken, NJ: John Wiley & Sons.

da Silva, G., Bozzelli, J. W., Liang, L., & Farrell, J. T. (2009). Ethanol Oxidation: Kinetics of the α-Hydroxyethyl Radical + O2 Reaction. *The Journal of Physical Chemistry A*, *113*(31), 8923–8933. https://doi.org/10.1021/jp903210a

Singh, E., Shankar, V. S. B., Tripathi, R., Pitsch, H., & Sarathy, S. M. (2018). 2-Methylfuran: A bio-derived octane booster for spark-ignition engines. *Fuel*, *225*, 349–357. https://doi.org/https://doi.org/10.1016/j.fuel.2018.03.169

Sivaramakrishnan, R., & Michael, J. V. (2009). Rate Constants for OH with Selected Large Alkanes: Shock-Tube Measurements and an Improved Group Scheme. *The Journal of Physical Chemistry A*, *113*(17), 5047–5060. https://doi.org/10.1021/jp810987u

Somers, K. P., Simmie, J. M., Gillespie, F., Conroy, C., Black, G., Metcalfe, W. K., et al. (2013). A comprehensive experimental and detailed chemical kinetic modelling study of 2,5-dimethylfuran pyrolysis and oxidation. *Combustion and Flame*, *160*(11), 2291–2318. https://doi.org/https://doi.org/10.1016/j.combustflame.2013.06.007

Splitter, D., Pawlowski, A., & Wagner, R. (2016). A Historical Analysis of the Co-evolution of Gasoline Octane Number and Spark-Ignition Engines. *Frontiers in Mechanical Engineering*, *1*. https://doi.org/10.3389/fmech.2015.00016

Storey, J. M. E., Curran, S. J., Lewis, S. A., Barone, T. L., Dempsey, A. B., Moses-DeBusk, M., et al. (2016). Evolution and current understanding of physicochemical characterization of particulate matter

from reactivity controlled compression ignition combustion on a multicylinder light-duty engine. *International Journal of Engine Research*, *18*(5–6), 505–519. https://doi.org/10.1177/1468087416661637

Stranic, I., Pang, G. A., Hanson, R. K., Golden, D. M., & Bowman, C. T. (2014). Shock Tube Measurements of the Rate Constant for the Reaction Ethanol + OH. *The Journal of Physical Chemistry A*, *118*(5), 822–828. https://doi.org/10.1021/jp410853f

Suarez-Bertoa, R., Zardini, A. A., Platt, S. M., Hellebust, S., Pieber, S. M., El Haddad, I., et al. (2015). Primary emissions and secondary organic aerosol formation from the exhaust of a flex-fuel (ethanol) vehicle. *Atmospheric Environment*, *117*, 200–211. https://doi.org/https://doi.org/10.1016/j.atmosenv.2015.07.006

Szybist, J. P., Busch, S., McCormick, R. L., Pihl, J. A., Splitter, D. A., Ratcliff, M. A., et al. (2021). What fuel properties enable higher thermal efficiency in spark-ignited engines? *Progress in Energy and Combustion Science*, *82*, 100876. https://doi.org/https://doi.org/10.1016/j.pecs.2020.100876

Tregrossi, A., & Ciajolo, A. (2010). Spectral Signatures of Carbon Particulate Evolution in Methane Flames. *Combustion Science and Technology*, *182*(4–6), 683–691. https://doi.org/10.1080/00102200903466517

Tripathi, R., Burke, U., Ramalingam, A. K., Lee, C., Davis, A. C., Cai, L., et al. (2018). Oxidation of 2-methylfuran and 2-methylfuran/n-heptane blends: An experimental and modeling study. *Combustion and Flame*, *196*, 54–70. https://doi.org/https://doi.org/10.1016/j.combustflame.2018.05.032

Trump, E. R., & Donahue, N. M. (2014). Oligomer formation within secondary organic aerosols: equilibrium and dynamic considerations. *Atmospheric Chemistry and Physics*, *14*(7), 3691–3701. https://doi.org/10.5194/acp-14-3691-2014

Vandergrift, G. W., Shawon, A. S. M., Dexheimer, D. N., Zawadowicz, M. A., Mei, F., & China, S. (2022). Molecular Characterization of Organosulfate-Dominated Aerosols over Agricultural Fields from the

Southern Great Plains by High-Resolution Mass Spectrometry. *ACS Earth and Space Chemistry*, *6*(7), 1733–1741. https://doi.org/10.1021/acsearthspacechem.2c00043

Vasudevan, V., Davidson, D. F., & Hanson, R. K. (2005). High-Temperature Measurements of the Reactions of OH with Toluene and Acetone. *The Journal of Physical Chemistry A*, *109*(15), 3352–3359. https://doi.org/10.1021/jp0501143

Wang, H. (2011). Formation of nascent soot and other condensed-phase materials in flames. *Proceedings of the Combustion Institute*, *33*(1), 41–67. https://doi.org/10.1016/j.proci.2010.09.009

Waqas, M. U., Hoth, A., Kolodziej, C. P., Rockstroh, T., Gonzalez, J. P., & Johansson, B. (2019). Detection of low Temperature heat release (LTHR) in the standard Cooperative Fuel Research (CFR) engine in both SI and HCCI combustion modes. *Fuel*, *256*, 115745. https://doi.org/https://doi.org/10.1016/j.fuel.2019.115745

Westbrook, C. K. (2000). Chemical kinetics of hydrocarbon ignition in practical combustion systems. *Proceedings of the Combustion Institute*, *28*(2), 1563–1577. https://doi.org/https://doi.org/10.1016/S0082-0784(00)80554-8

Westbrook, C. K., Mehl, M., Pitz, W. J., Kukkadapu, G., Wagnon, S., & Zhang, K. (2018). Multi-fuel surrogate chemical kinetic mechanisms for real world applications. *Physical Chemistry Chemical Physics*, *20*(16), 10588–10606. https://doi.org/10.1039/C7CP07901J

Wheeler, R. W., Downs, D., & Walsh, A. D. (1948). “Knock” in Internal Combustion Engines. *Nature*, *162*(4127), 893–894. https://doi.org/10.1038/162893a0

Whelan, C. A., Eble, J., Mir, Z. S., Blitz, M. A., Seakins, P. W., Olzmann, M., & Stone, D. (2020). Kinetics of the Reactions of Hydroxyl Radicals with Furan and Its Alkylated Derivatives 2-Methyl Furan and 2,5-Dimethyl Furan. *The Journal of Physical Chemistry A*, *124*(37), 7416–7426. https://doi.org/10.1021/acs.jpca.0c06321